Compliant Peg-in-Hole Assembly Using a Very Soft Wrist

Qi Zhang, Zhengtao Hu, Weiwei Wan and Kensuke Harada

***Abstract*— This paper proposes to use a high-compliance soft wrist to improve the performance of robotic peg-in-hole in uncertain environments. In contrast to past research in this field, in which force control with relatively low compliance has been used, we propose a method that searching and aligning motions can be easily realized by taking advantage of high compliance wrist under gravity. Our proposed PiH strategy is completely passive: After the peg is trapped into the hole during the hole-searching process using the spherical helix trajectory, it is guaranteed that the peg can automatically be inserted into the hole due to the effect of gravity and wrist compliance if the configuration of the peg is included in the no-escapable area. The no-escapable area can be obtained based on the potential analysis considering the contact state combined with the wrist compliance space. The effectiveness of the proposed method is experimentally verified by using the peg with various shapes and sizes.**

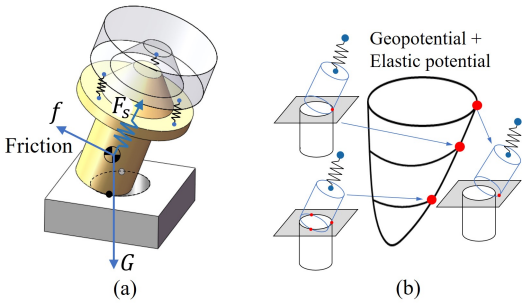

Fig. 1. (a) The soft wrist allows the peg to easily adapt to the constraint formed by the hole edge. The peg can slide toward the hole under the influence of gravity. (b) The sum of potential energy forms a configuration space. The peg's pose tends to change if the total potential can be smaller.

I. Introduction

Assembly tasks play a critical role in the overall production process, while the peg-in-hole (PiH) is one of the critical elements frequently used in an assembly task [1]. The PiH is challenging due to the uncertainties in the geometrical relation between a peg and a hole [2]. If the uncertainty is large, it becomes difficult for a robot to automatically identify the position of the hole and insert the peg into the hole.

Compliant wrists have been introduced to cope with the uncertainties in the geometrical relation between the peg and hole of the PiH tasks [3], [4]. For the small uncertainty, the wrists with low compliance can be used. However, there have been no wrist devices that can cope with the insertion tasks under large uncertainty. Two general approaches are applied to implement PiH by introducing compliance: the active compliance control and the passive compliance devices. Active compliance control can mimic the mechanical behavior of springs by using the feedback of a six-dimensional force/torque sensor [5], [6]. However, it is often difficult to perform high compliance by using the active compliance control due to the limited bandwidth of the servo controller [7]. In addition, when using force/position hybrid control to search the hole, the completion time cannot be estimated because the initial position deviation is random.

Remote center compliance (RCC) is a mechanical device that can prevent jamming when a peg is inserted into a hole with small clearance [8], [9], [10]. Using RCC, a peg can rotate passively around a remote center to reduce angular and lateral errors [11]. However, the general RCC devices can not adapt to situations with relatively large errors. It is required to develop passive compliance devices to overcome large uncertainty.

A high-compliance wrist device with three parallel springs was introduced in assembly task [12]. In addition, it was experimentally proved by using reinforcement learning that the high-compliance wrist can implement PiH tasks under large uncertainty [13]. However, the peg swings violently due to the absence of external dampers on the wrist. We propose installing soft dampers on the wrist to address the vibration issue. Furthermore, instead of using machine learning methods, we analyze the mechanism of utilizing high compliance to eliminate the high uncertainty and propose a corresponding insertion strategy.

So far, some novel passive peg-insertion strategies have been proposed using environmental constraints. Park et al. proposed in [14]that the peg can be kicked toward the hole when the contact state between the peg and the hole is two-point contact. Similarly, Hong et al. proposed an "attractive region" concept in [15], which is a constrained region formed by a peg and a hole. The bottom of the region refers to three-point contact. When a vertical force is applied to a tilted peg with a fixed tilt angle, the peg can passively move downward and realize three-point contact with the hole [14]. However, the attraction region only considers the translation of the peg. If both the translation and rotation of the peg are taken into consideration, the attraction region cannot be established solely by the environmental constraints. In our work, we address this issue by creating a configuration space of potential energy, which includes geopotential and elastic

Qi Zhang, Weiwei Wan are with the Graduate School of Engineering Science, Osaka University, Toyonaka, Osaka 560-0045, Japan (zhangqicurrent@gmail.com). Zhengtao Hu is with the School of Mechatronic Engineering and Automation, Shanghai University, Shanghai 200444, China, and also with the Graduate School of Engineering Science, Osaka University, Toyonaka, Osaka 560-0045, Japan. Kensuke Harada is with the Graduate School of Engineering Science, Osaka University, Toyonaka, Osaka 560-0045, Japan, and also with the National Institute of Advanced Industrial Science and Technology (AIST), Tokyo 100-8921, Japan.

potential. The peg can autonomously move and rotate to minimize the potential energy.

In this paper, we propose a mechanism for a very soft wrist and an insertion strategy. We also indicate that the peg cannot escape from the hole during the hole-searching motion under specific conditions. We extend the concept of "attractive region" by potential analysis to explain the condition. The soft wrist combining soft dampers allows the peg to move within a wide range, effectively compensating for large deviations and enabling quick stabilization. As for the insertion strategy, we introduce a hole-searching approach and an aligning approach. In the searching approach, a robot drags a peg and moves along a spherical helix trajectory while the peg tilts in various directions. When the peg tilts toward the hole, it can slide toward the hole passively under gravity until trapped, as depicted in Fig. 1(a). Thus, we call the approach "self-adaptive hole searching". In addition, we introduce no-escapable conditions by potential analysis to prevent the trapped peg from escaping from the hole. As shown in Fig. 1(b), for a system consisting of a spring and a peg, an attractive region can be established by potential energy. Just as water does not actively flow uphill, the trapped peg cannot escape from the hole if the potential energy tends to increase. Therefore, the search time is constant because the robot does not need to pause during the search motion. In the aligning approach, a force sensor is used to read the direction of the hole. The robot then moves toward the direction to reduce the large angular deviation and avoid jamming.

In the experiment part, we show hole-searching performance under a large positional deviation. We also compare the search time between using the proposed method and hybrid position/force control.

This paper presents two main contributions:

1) An insertion strategy using a soft wrist is proposed, including two approaches: self-adaptive hole searching and peg aligning.
2) We extend the concept of "attractive region" by creating a configuration space of potential and use it to explain no-escapable condition.

The paper is organized as follows: Section II introduces the structure of the soft wrist. Section III explains the insertion strategy. In Section IV, we experiment to illustrate the validity of the proposed strategy. Section V is the conclusion.

II. Mechanical Structure

A. Mechanism of the high-compliance device

This section explains our wrist device used for PiH tasks. The wrist can switch between compliant and stiff modes. In the compliant mode, a soft wrist can provide a large compliance space for a peg to move freely, as shown in Fig. 2. In the stiff mode, the compliance of the wrist can be disregarded.

The wrist consists of two parts: a gripper-side part(GSP) and an arm-side part(ASP). A cylinder is mounted on the top of the ASP. The two parts connect through a string, three extension springs, and three soft dampers. The springs

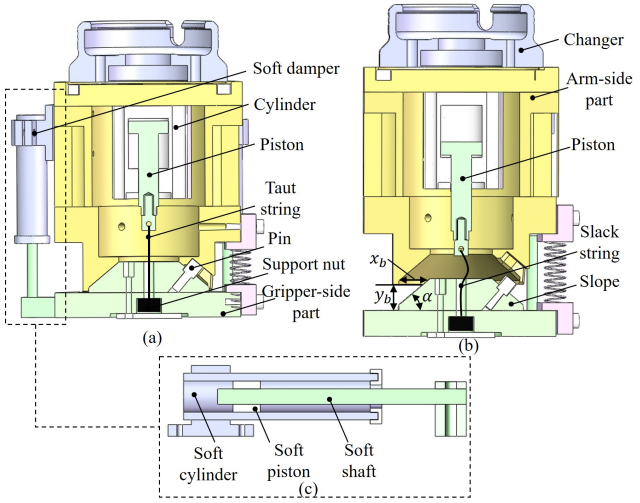

Fig. 2. (a) Stiff mode of the the wrist. (b) Compliant mode of the wrist. (c) Cross-section view of the soft damper.

and dampers are arranged in a circle. In the stiff mode, the cylinder contracts, causing the two parts to fit tightly together. The conical frustum structure, along with a pin, constrains the relative pose of the GSP. In the compliant mode, the cylinder expands, and the string becomes slack.

The PiH tasks are implemented by using the wrist in the compliant mode. The peg can slide toward a hole passively under gravity due to the large compliance space of the soft wrist. The boundary of the space in two directions are indicated by x_b and y_b, as shown in Fig. 2(b). The maximum value of them is x_{max} and y_{max}. y_{max} is determined by the spring stiffness k and the weight of the connected gripper. y_b and x_b can be adjusted by moving the wrist downward a distance of l_p to press the springs.

B. Soft damper structure

The soft wrist still has an issue that a gripper will swing for a long time when the wrist switches from stiff to compliant mode. The swinging can cause several problems. First, it can increase the deviation between the peg and the hole. Second, the large kinetic energy of the swing may damage the peg when it collides with the environment. Lastly, the gripper's swinging makes it challenging to obtain reliable measurements by sensors. General piston-type dampers can be used to dissipate vibration energy, but they will also constrain the compliance space of the soft wrist. In [16], the authors designed a soft damper to quickly stabilize a soft actuator. Such a soft damper is firstly used on the soft wrist to absorb oscillation energy without constraining the free movement of the GSP.

The soft damper consists of three parts: a soft cylinder, a soft shaft, and a soft piston, as shown in Fig. 2(c). The piston is fixed on the shaft, and its diameter fits with the inner diameter of the cylinder. The interior surface of the cylinder is lubricated to provide sliding friction. For the damper in this paper, the soft cylinder is a 12mm polyurethane tube, and the soft cylinder is a 4mm polyurethane tube.

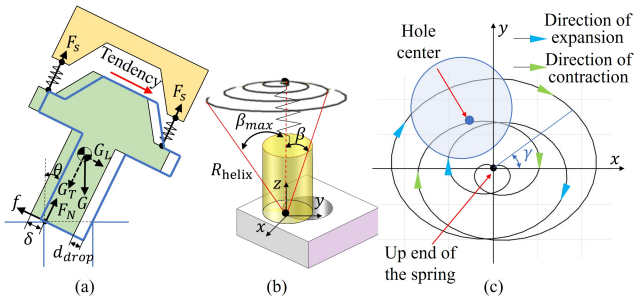

Fig. 3. (a) Force diagram of the tilted peg and wrist. (b) The spherical helix path of the robot arm. The rotation radius is R_{helix}. Tilt angle β increase to β_{max} and then decrease to zero. (c) Top view of the helix path.

III. Insertion Strategy using the Soft Wrist

The proposed insertion process is divided into three main steps: hole-searching, aligning the peg, and inserting the peg into the hole. For the first step, a self-adaptive hole-searching approach is proposed. We analyze the mechanism of the approach by force and potential analysis. In the aligning step, the F/T sensor is used to determine the position of the hole and the wrist moves toward the direction to reduce the angular deviation. In the insertion step, the wrist only needs to move downward. We assume no grasping error exists. In other words, the peg can be accurately grasped at the center of the gripper. Before the insertion motion, there is a positional deviation δ between the peg and the hole centers.

A. Hole-searching strategy

1) Analysis of hole-searching using the soft wrist: The mechanism of self-adaptive hole searching is illustrated in a 2-dimensional diagram, as shown in Fig. 3(a). To simplify the calculation, we assume that the tilt angle of the upper part of the wrist is approximately equal to that of the peg, which is θ. When the wrist is tilted toward the hole, the movement of the peg is affected by the gravity of the gripper G, support force F_N, frictional force f, and spring force F_s.

For a tilted peg, G can be divided into two components: G_L and G_T. As the tilt angle θ increases, G_L increases while G_T decreases. The decrease in G_T leads to a reduction of F_N and maximum static friction force. When G_L exceeds f, the peg will slide toward the hole, as indicated by the red arrow in Fig. 3(a). If the side surface of the peg comes into contact with the hole's edge, we consider the hole-searching motion to be successful. To achieve it, the compliance space needs to be large enough to compensate for the large positional deviation. Thus x_b of the compliance space needs to meet:

$$x_b \geq d_{drop} = 2R \cdot \cos\theta - 2\mathrm{R} + \delta \tag{1}$$

where R is the radius of the hole, θ is the tilt angle of the peg.

According to the equilibrium condition of spring forces and gravity, for a two-dimensional model as shown in Fig. 3(a), the spring's stiffness k can be calculated:

$$k = \frac{G}{2y_{max}} = \frac{G}{2(x_b + l_p) \cdot \tan\alpha} \tag{2}$$

In this work, we aim to compensate for the positional deviation(less than 9mm) by using the proposed hole-searching method. The design parameters of the soft wrist structure are chosen as follows: y_{max} is 11mm, α is 45°, and the height of the conical frustum is 12mm. We use the Robotiq Hand-E as the gripper, and its mass is 1.2kg. The stiffness of the springs is calculated to be 320N/m.

2) Searching trajectory: It is analyzed that a peg can slide passively to search a hole when the peg tilts toward the hole. Since the position of the hole relative to the peg is unknown, the wrist should be tilted traversing the entire direction. Hence, we suggest using a spherical helix trajectory to search the hole, as shown in Fig. 3(b). The radius R_{helix} is the distance from the peg's bottom center to the robot's wrist center. As the robot follows this path, the peg will tilt in various directions accordingly. To implement the aligning motion afterward, the tilt angle β increases gradually to the maximum value β_{max}, then gradually decreases to zero. The top view of the path is shown in Fig. 3(c). The expression of the trajectory is as follows:

$$\begin{aligned} x_i &= R_{helix} \cdot \sin\beta_i \cdot \sin\gamma_i \\ y_i &= R_{helix} \cdot \sin\beta_i \cdot \cos\gamma_i \\ z_i &= R_{helix} \cdot \cos\beta_i \end{aligned} \tag{3}$$

where

$$\begin{aligned} &\beta_i = \beta_{i-1} + \delta\beta \quad i \leq \frac{\beta_{max}}{\delta\beta} \\ &\beta_i = \beta_{i-1} - \delta\beta \; if \; \frac{\beta_{max}}{\delta\beta} < i \leq \frac{2\beta_{max}}{\delta\beta} \\ &\gamma_i = \gamma_{i-1} + \delta\gamma \\ &\delta\beta = \frac{2\beta_{max}}{i}, \; \delta\gamma = \frac{n \cdot 2\pi}{i}, \; n \geq 2 \end{aligned} \tag{4}$$

If the robot is controlled to follow this trajectory, no matter where the hole is located, there will be a moment when the peg tilts toward the hole. Then, the peg can be guided to slide toward the hole and trapped by the hole. It is worth noting that a high coefficient of friction at the contact point can hinder the peg's sliding motion. In this case, a larger β_{max} is required, and the search time will also increase accordingly.

3) No-escapable condition: In the general hole-searching method, the robot must often determine whether the hole has been found during the hole-searching process. The moment can be detected by monitoring the positional change of the end-effector. Once the hole has been found, the robot should immediately stop the searching motion to prevent the peg from escaping the hole. The escape phenomenon occurs due to the imbalance between the lateral force and the downward force exerted on the peg. If the lateral force is too large, the peg will escape from the hole, resulting in the failure of the insertion tasks [17]. Moreover, for the blind searching

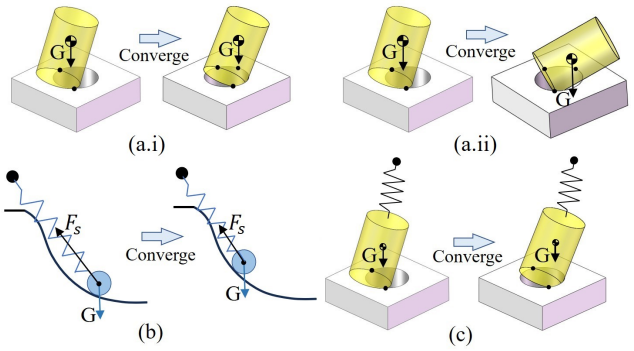

Fig. 4. (a.i) The peg can converge to three-point contact when the tilt angle is fixed. (a.ii) The peg may fall down if the tilt angle is not fixed. (b) Motion of a ball placed in a hemispheric environment under the effect of gravity and spring force. (c) Motion of a peg under the effect of gravity and spring force.

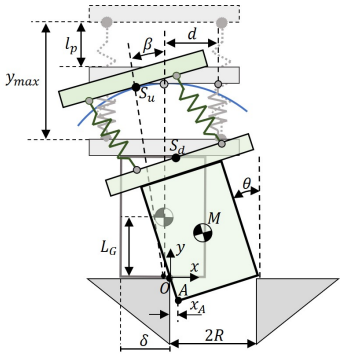

Fig. 5. The two-dimensional model of the peg, hole, and soft wrist. The grey blocks represent the initial position of the upper part and the peg, while the green blocks depict the posture of the upper part and the peg, assuming the peg has been trapped by the hole.

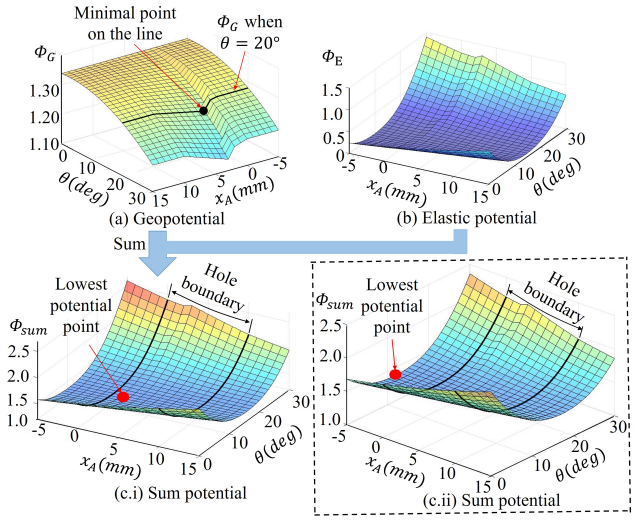

Fig. 6. (a) Geopotential field, (b) Elastic potential field, (c.i) Sum potential field when l_p is 3mm. (c.ii) Sum potential field when l_p is 1mm.

approach, the search time varies significantly depending on the positional deviations. Thus, accurately predicting the completion time of the assembly process is difficult [18].

In our strategy, if the soft wrist and the spherical helix path are used, it is unnecessary to sense the moment when the hole has been found. The robot simply needs to complete the entire hole-searching trajectory without pause, as the peg cannot escape from the hole under certain conditions. We call it the no-escapable condition. The no-escapable conditions are explained by using the concept of "attractive region".

In [14], [19], Qiao et al. proposed a theory called the "attractive region in environment" (ARIE). In PiH tasks, ARIE is a convex-shaped constrained region formed by the hole's edge. Regardless of the peg's initial position, it will eventually converge to a three-point contact state when the tilt angle is fixed, as shown in Fig. 4 (a.i). However, the rotation of the peg is not taken into consideration. If the peg can translate and rotate freely, the peg may tend to fall down, as shown in Fig. 4 (a.ii). Thus the attractive region cannot be formed only by the environment constraints in this case.

In this paper, we extend the concept of the attractive region and apply it to explain the no-escapable condition. When the position and orientation of the peg are both adjustable, the final pose of the peg is determined by the potential of the system. To illustrate it, we use the analogy of a small ball connected to a spring and placed in a hemispheric environment, as shown in Fig. 4(b). In this case, the attractive region cannot be formed solely by environmental constraints. However, the ball can still converge to a specific position under gravity, friction, and spring force. The final position is determined by the total potential Φ_{sum}, which is the sum of the elastic potential Φ_E and the geopotential Φ_G. When the up end of the spring moves within a specific range, if the ball remains within the hemispheric space under the minimum potential, the ball will not escape from the hole. We call the specific range the "no-escapable condition".

Similarly, for the peg in Fig. 4(c), the final pose of the peg depends on where Φ_{sum} is at its lowest value. There is a specific range that when the upper part of the spring moves within this range, the peg trapped by the hole will not escape from the hole. The range can be determined by the potential analysis, as explained below.

Fig. 5 presents the two-dimensional model of the peg, hole, and soft wrist. The wrist is simplified by two springs. If the peg has been trapped by the hole, the peg is most likely to escape from the hole when the wrist tilts toward the opposite direction of the hole. Therefore, we analyze the critical tilt angle of the ASP for this moment.

The tilt angle of the wrist is β, the tilt angle of the peg is θ, the distance from the center of mass to the bottom of the peg is L_G, the distance between the spring and wrist center is d, the initial positional deviation between the peg and the hole is δ, and the lowest point of the peg is designated as point A. The horizontal distance between point A and the origin (point O) is x_A. The wrist needs to move downward for a distance l_p to press the spring after the peg has contracted with the hole surface. The pressing motion is necessary to maintain the contact between the peg and the hole surface during the hole-searching motion.

The total potential of the system includes the gravitational and elastic potential, which can be expressed as:

$$\begin{aligned}\Phi_{sum} &= \Phi_G + \Phi_E \\ &= 0.5k \cdot \Delta l_{lftspr}^2 + 0.5k \cdot \Delta l_{rgtspr}^2 + G \cdot y_M\end{aligned} \tag{5}$$

where k is the stiffness of the spring, and y_M is the y-coordinate of the mass center. And Δl_{lftspr} is the extension length of the left spring, Δl_{rgtspr} is the extension length of the right spring, which can be calculated by the geometrical relationship of the peg and soft wrist:

$$\{\Delta l_{lftspr}, \Delta l_{rgtspr}\} = f(x_A, y_A, \theta, \beta, d, l_o, l_p, L_G) \tag{6}$$

where l_o is the original length of the spring.

The optimization used to find the position and tilt angle of the peg can in general be written as

$$\text{minimize :} \Phi_{sum}(x_A, y_A, \theta) \tag{7}$$

subject to the environment constraints:

$$y_A = \begin{cases} 0 & x_A < 0 \ or \ x_A > 2R \\ -x_A \tan\theta & 0 \le x_A < 2R\sin^2\theta \\ y_A = -(2R - x_A) \cdot \tan\theta & 2R\sin^2\theta < x_A < 2R \end{cases} \tag{8}$$

For a specific value of β, δ and l_p, if $x_A \in [0, 2R]$ when Φ_{sum} is minimal, the peg will not escape from the hole.

Fig. 6 illustrates the potential energy profile under the parameters of the soft wrist, l_p is 3mm, β is 15°, R is 5mm, and the deviation δ is 4mm. The geopotential and the elastic potential under the different x_A and θ are calculated, and their results are shown in Fig. 6(a) and (b). Then, the sum potential of the system can be obtained as shown in Fig. 6(c.i). The boundary of the hole is $0 \le x_A \le 10\text{mm}$.

According to Fig. 6(a), it can be observed that if θ remains constant and x_A varies, represented by the black line, a minimum point exists. And the peg tends to move towards the point. However, the geopotential decreases with the increase of θ. Therefore, an attractive region cannot be established solely by geopotential if both position and angle are variable. After adding elastic potential, in the sum potential field (Fig. 6(c.i)), a minimal point exists. Through this method, an attractive region consisting of both positional and tilt angle dimensions is established.

According to the results, the point of minimum potential energy is located within the hole. Therefore, under these conditions, as long as β does not exceed 15°, the trapped peg cannot escape from the hole. Under the same conditions, when the downward distance l_p is 1mm, the calculated sum potential field is shown in Fig. 6(c.ii). The minimal point of the potential field is located outside the hole boundary. In this case, the peg may escape from the hole. Therefore, increasing l_p can help prevent escaping when the no-escapable condition is not met. Based on the analysis, we can accurately estimate the assembly completion time because robots do not need to pause during the hole-searching process.

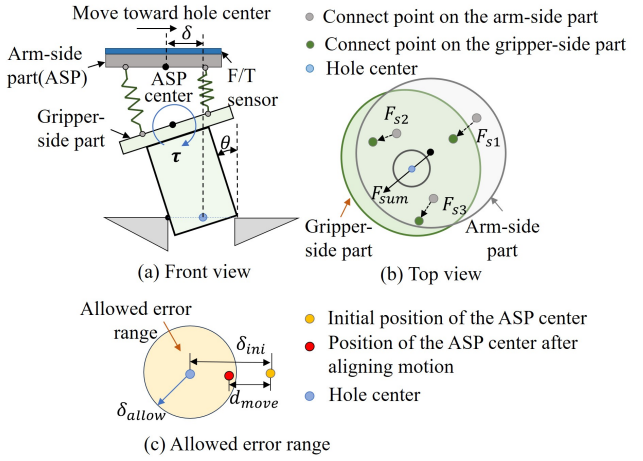

Fig. 7. (a) The two-dimensional model of the peg and wrist before the aligning motion. (b) The top view of the arm-side part and the gripper-side part. (c) The schematic diagram of the aligning motion.

B. Aligning strategy

After the searching motion, we assume the hole has trapped the peg. Due to positional deviation, the axis of the peg and the hole are not collinear, bringing an angular deviation θ, as shown in Fig. 7(a). Obviously, θ will decrease when the robot moves toward the hole center. Therefore, it is important to determine the moving direction and moving distance for the alignment strategy.

The moving direction can be determined by the force sensor which is installed at the wrist. Due to the soft wrist, the force sensor measures the resultant spring force instead of contact forces between the peg and the hole. Fig. 7(b) shows the top view of the two parts of the soft wrist at this moment. Since the peg is tilted, the three spring forces have horizontal components, denoted by F_{s1}, F_{s2}, and F_{s3}, respectively. The resultant force of the three forces is F_{sum}. The magnitudes and directions of these three forces are unknown, so they are represented by dashed lines. However, elastic force is a type of conservative force, and conservative forces act in the direction of decreasing potential energy. When the projection of the center of the ASP coincides with the center of the hole, the lateral elastic potential energy is zero. Therefore, the direction of F_{sum} is toward the center of the hole. In this way, the position of the hole can be determined.

The moving distance is determined by analyzing the allowed positional deviation so that jamming can be avoided. Due to the inherent compliance of the soft wrist, when the projection of the center of the ASP is located within a circular range around the hole center, the peg can be inserted into the hole without jamming as long as the wrist moves downward. The radius of this circular range is defined as δ_{allow}, which is represented by the orange circle in Fig. 7(c). δ_{allow} is closely related to clearance and can be determined through experiments. If the initial position of the wrist, which is outside of this range, can be moved within the range through the aligning motion, the hole-inserting motion can be implemented successfully.

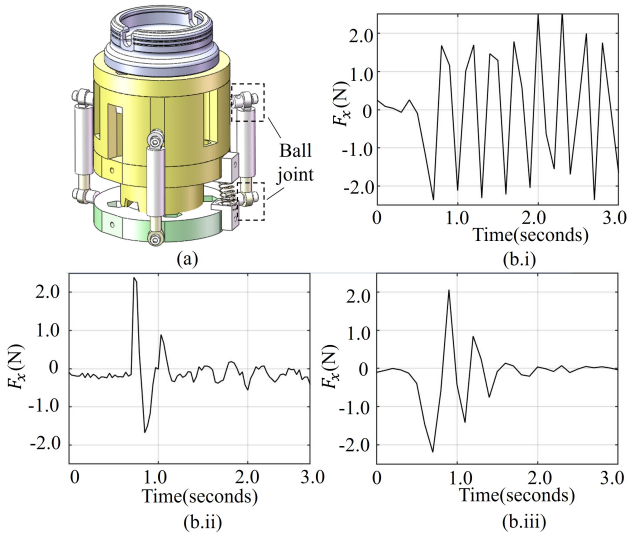

Fig. 8. (a) Soft wrist with piston-type dampers. (b.i) The change of F_x when dampers were not used. (b.ii) The change of F_x when the piston-type dampers with ball joints were installed on the soft wrist. (b.iii) The change of F_x when the soft dampers were installed on the soft wrist.

We assume that there is a maximum positional deviation δ_{max} between the initial position of the wrist center and the hole center. The initial positional deviation is δ_{ini}. The moving distance of the aligning motion is denoted as d_{move}. To avoid jamming during the inserting motion, the value of d_{move} should meet:

$$\forall \delta_{ini} \in [0, \delta_{max}] : \ |\delta_{ini} - d_{move}| \leq \delta_{allow} \tag{9}$$

It can be calculated from Eq. (9) that d_{move} and δ_{max} should satisfy:

$$d_{move} = \delta_{allow}, \ \delta_{max} \leq 2 \cdot \delta_{allow} \tag{10}$$

IV. Experiments

A. Performance of the self-adaptive hole searching

In this subsection, the performance of the self-adaptive hole searching is evaluated. The diameter of the peg is 10.0mm. The chamfer size is 0.2mm. The positional deviation between the peg and the hole is 9mm. l_p is 2mm, and β_{max} is 15°. The process of hole searching is shown in Fig. 9. It is demonstrated that the peg can rapidly slide toward the hole until trapped.

B. Performance of the damper

In this subsection, we evaluate the performance of swing attenuation using soft dampers, general piston-type dampers, and the absence of dampers. Piston-type dampers with ball joints at both ends were used to ensure that the gripper can still move within a large range, as depicted in Fig. 8(a). We tilted the gripper to a fixed angle of 20° and then released it. An F/T sensor is used to track force changes along the x-axis.

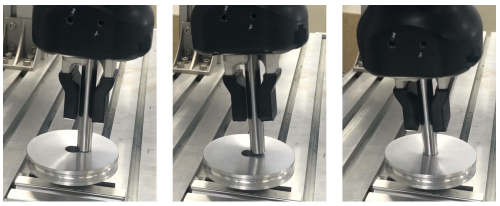

Fig. 9. Process of the self-adaptive hole searching. (a) A large deviation existed between the peg and the hole. (b) The peg tilted toward the hole. (c) The peg slid toward the hole and was trapped by the hole.

In Fig. 8(b.i), if dampers were not used, the gripper continued to oscillate without attenuation. In Fig. 8(b.ii), if the piston-type dampers were used, the swing amplitude of the gripper can be reduced rapidly in the beginning. However, the gripper still swings slightly for a long time. This is caused by the inevitable gap between the ball stud and bearing[20]. Using ball joints with minimal gaps can alleviate this issue but would be expensive. When the soft dampers were used, F_x began to oscillate at 0.5 seconds. The amplitude of the oscillation gradually decreased and stopped at 1.5 seconds. It is illustrated that the proposed soft dampers perform better in stabilizing the gripper.

C. Insertion experiment

In this part, we evaluated the performance of the proposed insertion strategy. We conducted experiments using a real robot to compare the completion time of using a soft wrist versus without it for completing the insertion task.

1) Using the soft wrist: We utilized a UR3e robot and a Robotiq Hand-E gripper to hold a peg with a diameter of 10.00mm and insert it into a hole with a diameter of 10.04mm. The chamber and the depth of this hole are 0.5mm and 10mm, respectively. Through experiments we found δ_{allow} is about 2mm for this clearance condition. Accordingly, the maximum initial δ_{max} is 4mm, and d_{move} is set as 2mm. l_p is set as 3mm, thus x_b can be calculated as 8mm. β_{max} of the spherical helix is set as 15° according to the calculated no-escapable condition in Sec.III-A-3.

The experimental process is shown in Fig. 10. In Fig. 10(a), the wrist moved downward and pressed the spring. Then, the wrist followed the spherical helix trajectory, as shown in Fig. 10(b). Under gravity, the peg slid toward the hole (Fig. 10(c)). After the robot arm completed the searching trajectory, the wrist returned to the initial position, while the peg was trapped by the hole, as shown in Fig. 10(d). At this time, the F/T sensor of the UR robot measured the force data in the x-y plane to determine the position of the hole. Then, the wrist moved 2mm horizontally toward the direction, as shown in Fig. 10(e). Finally, the wrist moved downward to complete the insertion motion, as shown in Fig. 10(f).

The insertion tasks of various components were also implemented, as shown in Fig. 11. The diameters of the circular parts are 19.90mm and 20.00mm. The chamfer size of the circular hole is 0.5mm. The depth of the hole is

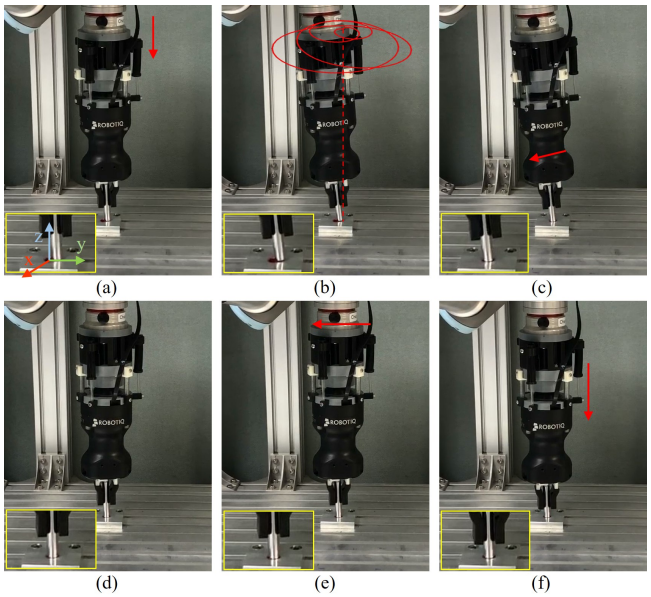

Fig. 10. The process of the insertion task using the soft wrist. (a) Approaching the hole. (b) Following the spherical helix trajectory. (c) The peg slid toward the hole. (d) Completed the searching motion. (e) Aligning the peg. (f) Inserting the peg into the hole.

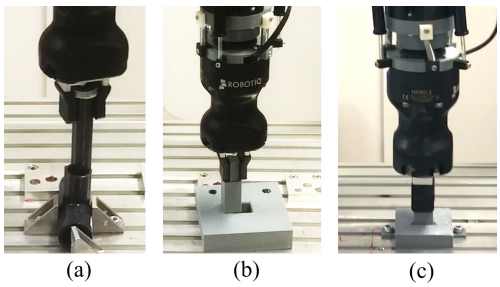

Fig. 11. (a) Insert a tube with a circular profile. (b) Insert a peg with a square profile, (c) Insert a peg with a triangular profile.

40mm. The diameters of the triangular parts are 21.10mm and 21.70mm. The depth and chamfer size of the triangular hole is 15mm and 2.5mm, respectively. The diameters of the square parts are 19.60mm and 20.00mm. The depth and chamfer size of the square hole is 15mm and 2mm, respectively. Insertion experiments of triangular components were conducted when the misalignment of the yaw angle is 10° and 15°. It was observed that the springs of the soft wrist can deform to compensate for a misalignment of the yaw angle when the misalignment of the yaw angle is not larger than 10°, as depicted in Fig. 11. These insertion tasks are demonstrated in the attached video.

2) Comparison with the traditional insertion methods: The force-position hybrid control and proposed strategy were applied to search the hole. The positional deviation between the peg and the hole was randomly set within the range of 0-8mm. Each method was conducted for fifteen trials, and their search time was recorded. Fig. 12 shows the frequency histogram of the search time. For the hybrid control method, the variance of search time is large. The average search time

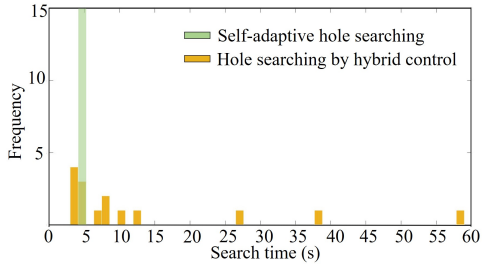

Fig. 12. Frequency histogram of the search time.

and standard deviation for the method are 13.20s and 16.01s, respectively. Such a large variance is caused by the random initial position deviation between the peg and the hole. In contrast, when using the proposed strategy, the searching motion can be completed with a constant time because the robot does not need to pause during the searching motion. For a smooth-surfaced peg, β_{max} was set as 7° and the search time was about 5s. For a rusted peg, β_{max} needs to be larger and was set as 12°. The search time was about 8s in this case.

TABLE I
COMPARISONS BETWEEN EXISTING RCCS AND OUR SOFT WRIST

Article	Stroke	Maximum initial deviation	Stiffness
[8]	2mm	1.5mm	$1.0 \times 10^3 N/m$
[9]	2mm	2mm	$3.5 \times 10^3 N/m$
[10]	-	2mm	$9.8 \times 10^4 N/m$
Ours	11mm	9mm	$3.2 \times 10^2 N/m$

For RCC devices and the soft wrist, although they both serve as wrist-like structures connecting the robot arm and the gripper through elastic components, they have three significant differences. Firstly, the two devices are used to solve different issues in different conditions. Most RCC devices are designed to avoid jamming during the insertion of the peg. In this case, the positional deviation is small thus robot only needs to move downward. For the soft wrist, it is used to search the hole when the position deviation is relatively large. In this case, the peg cannot be inserted into the hole directly. Secondly, their strokes have large differences. The soft wrist requires larger strokes to compensate for the larger deviations. Thirdly, unlike the RCC devices, the soft wrist does not have a compliant center. The comparison between existing RCC devices and our soft wrist is shown in Table.I.

D. The effect of stiffness of the soft wrist

This subsection discusses the impact of spring stiffness on hole-searching and hole-inserting motions. The selected spring stiffness are 320N/m, 420N/m, 560N/m, and 730N/m, respectively. In the hole-searching task, we compared the maximum allowable deviation that the peg does not escape from the hole. β is set as 10° and l_p is set as 3mm. For each stiffness, the experiments were repeated five times and

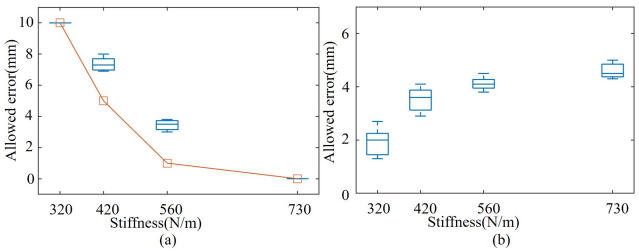

Fig. 13. (a) Box plots of allowed error that the peg cannot escape from the hole under the different stiffness. The orange curve is a theoretical value measured by the no-escapable condition. (b) Box plots of allowed error that jamming can be avoided under the different stiffness.

allowed errors were recorded. The boxplot of the results is shown in Fig. 13

Since the diameter of the hole is 10mm, the maximum allowable deviation is 10mm. It can be seen that the theoretical allowable deviation is not larger than the experimental value. This may be caused by the frictional force between the peg and the hole, which can prevent the peg from escaping. As the spring stiffness increases, the allowable deviation decreases. This indicates that if springs with larger stiffness are used, the peg may escape from the hole easily. However, if the tilt angle is set as a small value, the peg can hardly slide toward the hole. Therefore, a soft wrist with high stiffness is difficult to use to search the hole.

Fig. 13(b) shows the allowable deviation for the soft wrist with different stiffness under the no jamming condition. It can be seen that jamming is more likely to occur when the spring is relatively soft.

In summary, when the spring stiffness is large, it is not desired to search the hole, and when the spring stiffness is small, it is not desired to avoid jamming. One solution is to use variable stiffness springs. The spring stiffness can be adjusted to a small value during the hole-searching process and can be adjusted to a large value to avoid jamming during the inserting process.

V. Conclusion

We propose an insertion strategy using a very soft wrist installed with soft dampers to implement the insertion tasks under large deviations. The concept of "attractive region" is extended by creating a configuration space of potential to explain the no-escapable condition. The effectiveness of the proposed strategy has been validated through a series of insertion experiments. Nevertheless, the current hardware can only be used in vertical assembly tasks. The deviation of the load's mass center will increase the initial positional error. To address this issue, we are considering using springs with variable stiffness on the soft wrist in future work. The stiffness of each spring can be adjusted to correct the increased positional errors.

References

[1] C. Sloth, A. Kramberger, and I. Iturrate, "Towards easy setup of robotic assembly tasks," *Advanced Robotics*, vol. 34, no. 7-8, pp. 499–513, 2020.

[2] J. Navarro-Gonzalez, I. Lopez-Juarez, R. Rios-Cabrera, and K. Ordaz-Hernández, "On-line knowledge acquisition and enhancement in robotic assembly tasks," *Robotics and Computer-Integrated Manufacturing*, vol. 33, pp. 78–89, 2015.

[3] J. Yao, D. Cai, H. Zhang, H. Wang, D. Wu, and Y. Zhao, "Task-oriented design method and research on force compliant experiment of six-axis wrist force sensor," *Mechatronics*, vol. 35, pp. 109–121, 2016.

[4] J. Jiang, Z. Huang, Z. Bi, X. Ma, and G. Yu, "State-of-the-art control strategies for robotic pih assembly," *Robotics and Computer-Integrated Manufacturing*, vol. 65, p. 101894, 2020.

[5] J. Luo, E. Solowjow, C. Wen, J. A. Ojea, A. M. Agogino, A. Tamar, and P. Abbeel, "Reinforcement learning on variable impedance controller for high-precision robotic assembly," in *2019 International Conference on Robotics and Automation (ICRA)*, pp. 3080–3087, IEEE, 2019.

[6] Z. Hu, W. Wan, K. Koyama, and K. Harada, "A mechanical screwing tool for parallel grippers—design, optimization, and manipulation policies," *IEEE Transactions on Robotics*, vol. 38, no. 2, pp. 1139–1159, 2021.

[7] P. Pounds, R. Mahony, and P. Corke, "Modelling and control of a large quadrotor robot," *Control Engineering Practice*, vol. 18, no. 7, pp. 691–699, 2010.

[8] S. Joo, H. Waki, and F. Miyazaki, "On the mechanics of elastomer shear pads for remote center compliance (rcc)," in *Proceedings of IEEE International Conference on Robotics and Automation*, vol. 1, pp. 291–298, IEEE, 1996.

[9] U. Kim, D. I. Park, G. Jo, H. Jeong, H.-S. Kim, S.-H. Song, and C. Park, "Displacement sensor integrated into a remote center compliance device for a robotic assembly," *IEEE Access*, vol. 9, pp. 43192–43201, 2021.

[10] S. Lee, "Development of a new variable remote center compliance (vrcc) with modified elastomer shear pad (esp) for robot assembly," *IEEE Transactions on Automation Science and Engineering*, vol. 2, no. 2, pp. 193–197, 2005.

[11] D. E. Whitney *et al.*, "Quasi-static assembly of compliantly supported rigid parts," *Journal of Dynamic Systems, Measurement, and Control*, vol. 104, no. 1, pp. 65–77, 1982.

[12] F. von Drigalski, K. Tanaka, M. Hamaya, R. Lee, C. Nakashima, Y. Shibata, and Y. Ijiri, "A compact, cable-driven, activatable soft wrist with six degrees of freedom for assembly tasks," in *2020 IEEE/RSJ International Conference on Intelligent Robots and Systems (IROS)*, pp. 8752–8757, IEEE, 2020.

[13] M. Hamaya, K. Tanaka, Y. Shibata, F. Von Drigalski, C. Nakashima, and Y. Ijiri, "Robotic learning from advisory and adversarial interactions using a soft wrist," *IEEE Robotics and Automation Letters*, vol. 6, no. 2, pp. 3878–3885, 2021.

[14] R. Li and H. Qiao, "Condition and strategy analysis for assembly based on attractive region in environment," *IEEE/ASME Transactions on Mechatronics*, vol. 22, no. 5, pp. 2218–2228, 2017.

[15] H. Qiao, M. Wang, J. Su, S. Jia, and R. Li, "The concept of "attractive region in environment" and its application in high-precision tasks with low-precision systems," *IEEE/ASME Transactions on Mechatronics*, vol. 20, no. 5, pp. 2311–2327, 2014.

[16] F. Ni, A. Henning, K. Tang, and L. Cai, "Soft damper for quick stabilization of soft robotic actuator," in *2016 IEEE International Conference on Real-time Computing and Robotics (RCAR)*, pp. 466–471, IEEE, 2016.

[17] H. Park, J. Park, D.-H. Lee, J.-H. Park, M.-H. Baeg, and J.-H. Bae, "Compliance-based robotic peg-in-hole assembly strategy without force feedback," *IEEE Transactions on Industrial Electronics*, vol. 64, no. 8, pp. 6299–6309, 2017.

[18] M.-S. Choi, Y.-W. Shin, G.-R. Jang, D.-H. Lee, J.-H. Park, and J.-H. Bae, "Kinesthetic sensing for peg-in-hole assembly based on in-hand manipulation," *IEEE Robotics and Automation Letters*, vol. 6, no. 4, pp. 8418–8425, 2021.

[19] J. Xu, Z. Hou, Z. Liu, and H. Qiao, "Compare contact model-based control and contact model-free learning: A survey of robotic peg-in-hole assembly strategies," *arXiv preprint arXiv:1904.05240*, 2019.

[20] B.-H. Jang and K.-H. Lee, "Analysis and design of a ball joint, considering manufacturing process," *Proceedings of the Institution of Mechanical Engineers, Part C: Journal of Mechanical Engineering Science*, vol. 228, no. 1, pp. 146–151, 2014.